

# Effect of yttrium on the electrical and mechanical properties of in situ synthesized CNTs/CuCr composites

Liangyan Zhao<sup>1,b)</sup>, Xiaohong Chen<sup>1,a)b)</sup>, Ping Liu<sup>1</sup>, Wei Li<sup>1</sup>, Fengcang Ma<sup>1</sup>, Daihua He<sup>1</sup>, Jinzhang Li<sup>1</sup>

<sup>1</sup>School of Materials Science and Engineering, University of Shanghai for Science & Technology, Shanghai 200093, People's Republic of China

<sup>a)</sup>Address all correspondence to this author. e-mail: chenxiaohong5547@163.com

<sup>b)</sup>These authors contributed equally to this work.

Received: 1 December 2018; accepted: 21 March 2019

Addition of carbon nanotubes (CNTs) to copper materials significantly enhances their properties. However, the performance of CNTs/Cu composites is often not as good as expected mainly because of difficulties in controlling growth and uniform dispersion of CNTs in the matrix. Our study provides an effective way to prepare CNTs/CuCr and CNTs/CuCrY composites using chemical vapor deposition. The morphology and structure of these composites were characterized by scanning electron microscope, X-ray diffraction, X-ray photoelectron spectroscopy, and Raman spectroscopy to understand how Y incorporation affects properties of these composites. Our results showed that addition of 0.1 wt% Y enhances the catalytic properties of Cr and helps to obtain purer and pristine Cu substrate. We also studied tensile strength, electric conductivity, corrosion, and wear resistance of these composites. When Y was added, composite properties improved significantly. Tensile strength and corrosion resistance increased by 35.21 and 53.28%, respectively. Electric conductivity increased to 90.9% International Annealed Copper Standard and the coefficient of friction reduced to 0.3.

## Introduction

Copper-based composites are widely used in aviation, aerospace, electronics, etc. Search for smart composite materials motivates academic and industrial research and development to find materials with high strength and high conductivity. However, as the strength of copper-matrix composites increases, their electrical conductivity decreases. This phenomenon attracted significant scientific attention to copper matrix composites [1, 2]. Carbon nanotubes (CNTs) possess unique structural characteristics, electrical and mechanical properties, excellent electrical conductivity, and excellent high-temperature strength. Thus, all these properties make CNTs ideal reinforcement materials for preparation of high-strength and high-conductivity copper-based composites [3, 4, 5].

Walid [6] obtained CNTs/Cu composites by electroless plating. After spark plasma sintering (SPS), the electrical conductivity of CNTs/Cu composite was 72% International Annealed Copper Standard (IACS) and Vickers hardness and yield stress were up to 108 HV and 341.2 MPa, respectively. Shukla [7] blended CNTs and Cu powders by ball-milling

followed by sintering and achieved composites with a tensile strength equal to 330 MPa. However, the application of electroless plating [8] and powder metallurgy method [9] often results in poor wettability between CNTs and Cu, as well as which leads to structural instability of the obtained CNTs. Thus, these methods cannot ensure uniform dispersion of CNTs in Cu as well as reliable bonds between them.

In situ synthesis chemical vapor deposition (CVD) is one of the best methods for preparation of copper-based CNT composites. It is simple to implement (especially on a large scale) and operate, and it offers strong controllability and low cost [10, 11, 12]. Kang [13] used Ni catalyst to obtain CNTs dispersed in Cu originally prepared by powder metallurgy process and achieved good dispersion and interfacial bonding between CNTs and Cu. CNTs incorporation significantly improved hardness and yield strength of the composite materials. However, very active catalysts, such as Ni and Fe, demonstrate high solubility in Cu, which can significantly reduce electrical conductivity of the composites. The solubility of Cr in Cu is very limited, and thus Cr will not affect Cu

conductivity significantly [14]. Thus, in this work, we propose in situ synthesis of CNTs directly on Cu powder using 0.6 wt% Cr as a catalyst.

Despite these advantages, the catalytic activity of Cr is lower than that of Ni and Fe. Hence, enhancement of catalytic activity of Cr, which will also enable controllable growth of high-quality CNTs with uniform dispersion and minimum defects, is needed. One of the most critical factors influencing synthesis of CNTs by CVD is choice of a catalyst. Dispersion, activity, quantity, and size of the catalysts will influence distribution, yield, size, and structure of CNTs.

Florio [15] reported that  $Y_2O_3$  can stabilize the crystal structure of tetragonal zirconia. Kang [13, 16] studied in situ synthesis of CNTs on Cu and found that addition of Y can prevent Ni catalyst from forming solid solution with the Cu matrix and can also improve thermal stability of the catalyst. Thus, the addition of Y should increase temperature and time, at which the catalyst particles dissolved in the Cu matrix, ensuring structural stability of the catalyst in the reaction zone and maximized performance of a catalyst. Y is chemically very active, and its affinity for O, N, and S is much higher than that of Cu. Thus, it can bond with these elements before Cu and form inclusions in Cu-matrix [17, 18, 19]. We believe that this property will help to reduce the solubility of impurities in Cu to keep the matrix pristine. Thus, we added Y to improve catalytic performance, yield, and quality of synthesized CNTs, as well as overall and the properties of resulting composite material. The addition of 0.1 wt% Y can promote the precipitation of Cr in the aging process. At the same time, the composites obtained by this addition have the best mechanical properties and the least influence on the conductivity of composites [20, 21].

In this work, we added 0.1 wt% of Y as an additional catalyst with the goal to enhance performance of Cr and composites properties. Our experimental procedure included solution and aging treatment of CuCr and CuCrY alloy powders to achieve uniform precipitation of Cr on the composite surfaces to ensure an even growth of high-quality CNTs. Scanning electron microscope (SEM), transmission electron microscopy (TEM), X-ray diffraction (XRD), Raman spectroscopy, conductivity, and

friction tests were conducted to analyze the role of Y on catalytic activity of Cr and CNTs growth.

## Results and discussion

### Effect of Y on preparation of CNTs/CuCr composite powders with Cr as a catalyst

Figure 1 schematically shows in situ catalytically assisted CNT growth mechanism on Cu matrix. Cr particles are uniformly distributed on the matrix after solution and aging treatment. During CNT synthesis, C atoms, activated by  $C_2H_4$  cracking, are first adsorbed by the catalyst and then diffuse into it. After the catalyst, droplet becomes supersaturated with carbon, carbon starts precipitating from the bottom part of the catalyst droplet, and nucleates at the interface with the matrix-forming CNT. Catalyst particles are lifted upward as carbon continues to precipitate and form CNT. As the CNT growth continues, catalyst droplet detaches from the surface of the matrix staying at the top of a CNT [22, 23].

To determine the effect of Y on the surface morphologies of CuCr and CuCrY alloy powders, samples after solution and aging treatment as well as after in situ CNT growth, were analyzed using SEM (Fig. 2). Only a very small amount of catalyst particles precipitated on the surface of CuCr alloy powders after solution and aging treatment [Fig. 2(a)]. Catalytic activity was low, which resulted in low yield [Fig. 2(e)], uneven distribution, and poor morphology of the CNTs formed on the surface of CuCr alloy powders [Fig. 2(c)]. CuCrY alloy powders demonstrated a much more considerable number of fine and uniform precipitated catalyst particles with minimum impurities [Fig. 2(b)]. Addition of Y promoted the precipitation of Cr, improved its catalytic activity, and avoided the formation of unwanted carbon deposits during CNT growth. Moreover, the distribution of CNTs in the composite was very uniform and their walls were smooth and clean [Fig. 2(d)]. The yield of CNTs obtained with CuCrY alloys could reach 141% [Fig. 2(e)].

XRD patterns of both CNTs/CuCr and CNTs/CuCrY composite powders [Fig. 2(f)] demonstrated three strong peaks.

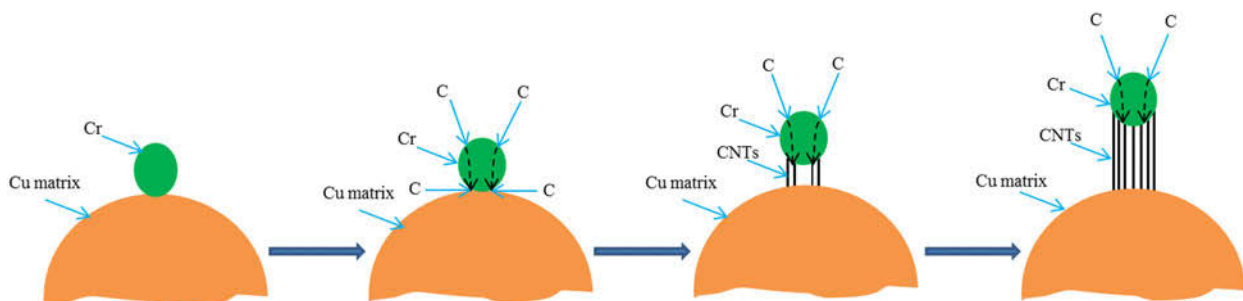


**Figure 1:** Schematics of catalytically assisted growth of CNTs.

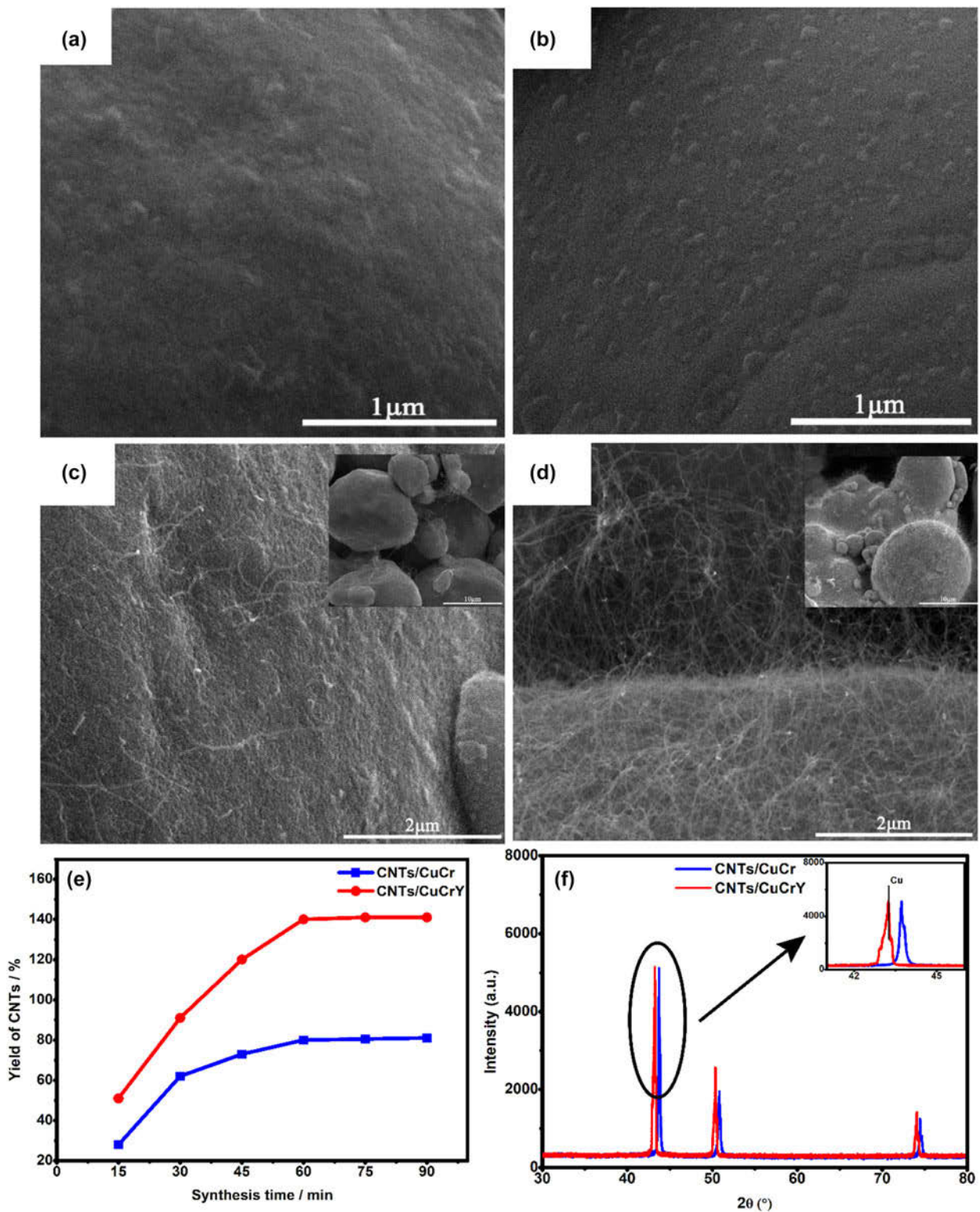


**Figure 2:** SEM micrographs of (a) CuCr and (b) CuCrY alloy powders after solution and aging treatment. High magnification SEM images of CNTs/CuCr (c) and CNTs/CuCrY (d) composite powders. Inserts in (c) and (d) show low-magnification SEM images of the corresponding composite powders. (e) Yield of CNTs obtained with CuCr and CuCrY alloys. (f) XRD spectra of CNTs/CuCr and CNTs/CuCrY composite powders. Insert shows enlarged peaks at  $\sim 43^\circ$ .

Positions of these peaks were very close for both composites. 2θ value corresponding to the strongest peak of the CNTs/CuCr composite powder was slightly shifted relative to the 2θ value of the Cu [see insert in Fig. 2(f)]. This indicates solution formation between Cr and Cu matrix [24]. The strongest peak of CuCrY was left-shifted and its position was in good agreement with the 2θ value of the same peak corresponding to metallic Cu, indicating reduction of Cr solubility in Cu matrix when Y was present. Thus, we believe the presence of Y also promoted aging precipitation of individual catalytic Cr particles instead of their solubility in Cu. No noticeable carbon peaks were observed in XRD patterns because of the very low CNT content. No diffraction peaks related to Y-phases were observed also because of small amount of Y in the composite powders.

X-ray photoelectron spectroscopy (XPS) measurements were carried out to investigate chemical compositions and oxidation states of CNTs/CuCr and CNTs/CuCrY composite powders (see Fig. 3). XPS wide scan spectrum exhibited peaks at different binding energies [see Fig. 3(a)]. The core-level spectra of Cu 2p for both composite powders are shown in Fig. 3(b). Peaks at 932.5 and 952.4 eV were assigned to Cu 2p<sub>3/2</sub> and Cu 2p<sub>1/2</sub>, respectively [25]. The sizes of satellite peaks indicate that CNTs/CuCr composite powders contained more CuO than CNTs/CuCrY composites. The presence of CuO will reduce electric conductivity of the material. Figures 3(c) and 3(d) show C 1s spectra of CNTs/CuCr and CNTs/CuCrY composite powders, respectively. C 1s spectra were fitted using a Gaussian–Lorentzian peak shape after performing a linear background correction. Peaks located at 284.8 and 285.6 eV were attributed to the sp<sup>2</sup>-hybridized and sp<sup>3</sup>-hybridized carbon atoms, respectively [26]. The relative atomic percentages of different carbon bonds were calculated from the corresponding peak areas in C 1s spectra. CNTs/CuCrY composite powders had higher percentage of sp<sup>2</sup>-hybridized carbon, indicating higher degree of graphitization and fewer lattice defects for the corresponding CNTs [27]. The core-level spectra of Y 3d for CNTs/CuCrY are shown in Fig. 3(e). Peaks at 156.85 and 185.85 eV were assigned to Y 3d<sub>5/2</sub> and Y 3d<sub>3/2</sub>, respectively, which correspond to Y<sub>2</sub>O<sub>3</sub> [28]. Y<sub>2</sub>O<sub>3</sub> acts as a stabilizer preventing diffusion between Cr catalyst and Cu matrix. Y<sub>2</sub>O<sub>3</sub> presence also improves temperature and time needed for Cr particles to dissolve in the Cu matrix, which ensures structural stability of the catalyst in the reaction zone.

### Y effect on properties of CNTs/CuCr composites

CNTs/CuCr and CNTs/CuCrY composites were prepared by SPS of CNTs/CuCr and CNTs/CuCrY composite powders. Figure 4 shows Raman spectra of both composites. Typical D and G bands characteristic to CNTs appeared at 1352.47 cm and 1596.69 cm<sup>-1</sup> [29], respectively. The intensity ratio of

these two bands (*I<sub>D</sub>/I<sub>G</sub>*) for CNTs/CuCr and CNTs/CuCrY composites were 1.106 and 0.922, respectively. Lower *I<sub>D</sub>/I<sub>G</sub>* ratios indicate better graphitic crystallinity of CNTs [30]. *I<sub>D</sub>/I<sub>G</sub>* ratio decreased (i.e., crystallization of CNTs increased) when Y was present. In addition, Raman peaks in the spectrum of CNTs/CuCrY composites were stronger, indicating higher CNT yield and quality after Y was added.

HRTEM was used to study interfacial bonding between CNTs and Cu in CNTs/CuCrY composites. CNTs exhibited smooth and clean walls [see Fig. 5(a)]. CNTs are tightly bound to the Cu matrix, and no significant physical gaps and intermediate compounds were observed in these micrographs [see Fig. 5(b)]. Thus, CNTs and Cu had tight interfaces in the composites.

Tensile tests were performed using densified samples. Figure 5(c) shows true tensile stress–strain curves for CuCr, CuCrY, CNTs/CuCr, and CNTs/CuCrY materials. After addition of Y, the strength of CuCrY and CNTs/CuCrY improved. The main reason of this improvement was the pinning effect of the dislocation formed between Y and Cu, which made it difficult for dislocation to move. The strengths of CNTs/CuCr and CNTs/CuCrY reached 297.4 and 402.1 MPa, respectively. Which we attributed to in situ grown CNTs formed a good interface with the Cu and CNTs can bear load with the substrate [31].

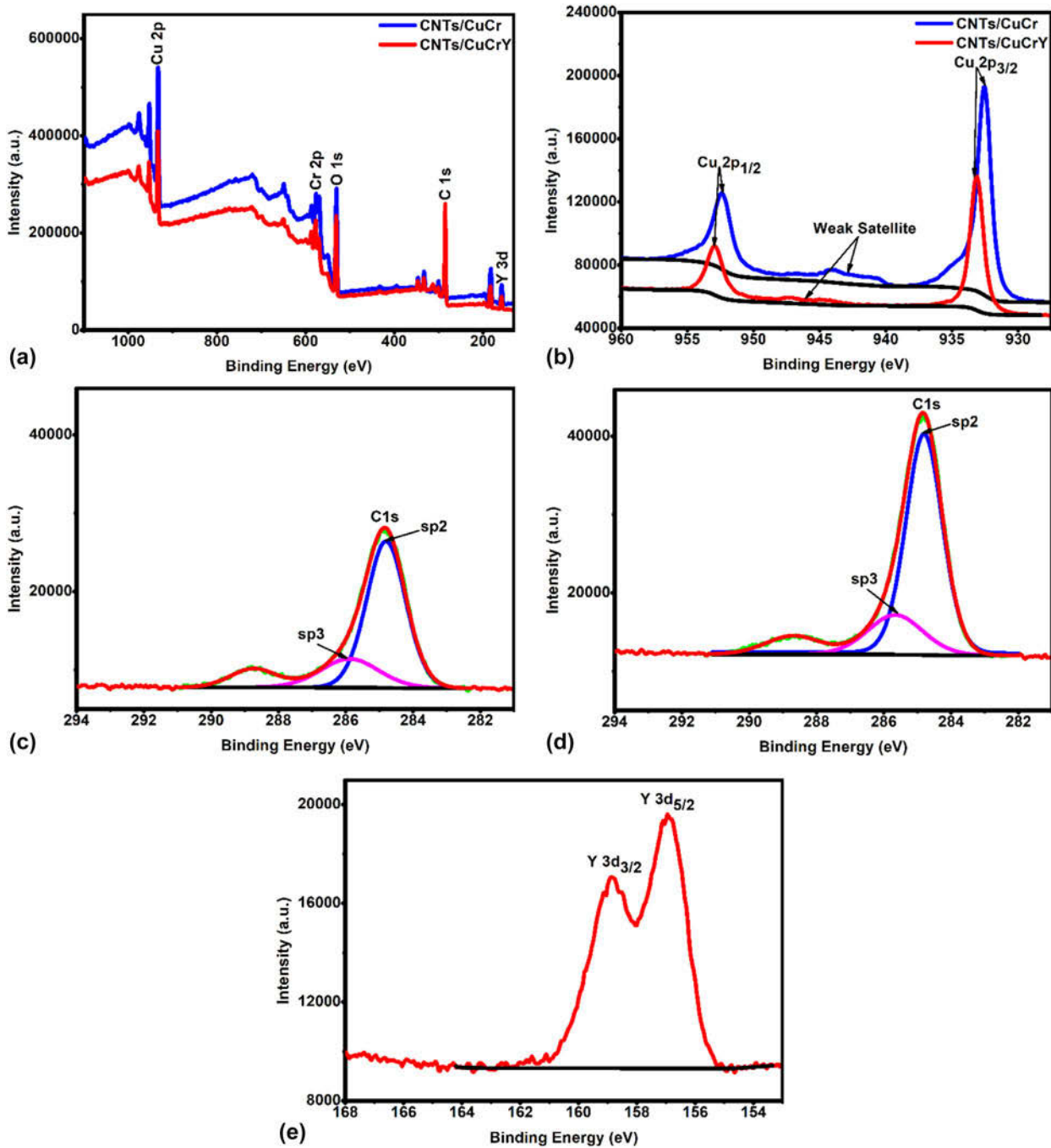
Table I lists tensile strength and conductivity of all samples. The addition of Y improved conductivity of the materials. The incorporation of Cr into Cu can cause lattice distortion and reduce Cu conductivity. The addition of Y can increase the amount of precipitated Cr and reduce Cr solubility in Cu, thus preventing negative impact of Cr on conductivity [32].

Figure 6 shows Tafel plots of the four composites (each area is 1 cm<sup>2</sup>) in 3.5 wt% NaCl solution. The polarization curve (*E<sub>corr</sub>*) of CuCrY and CNTs/CuCrY showed a considerable positive shift compared with the curves of CuCr and CNTs/CuCr, respectively. The corrosion current density (*I<sub>corr</sub>*) of CuCrY was significantly lower than that of CuCr. Moreover, corrosion current density (*I<sub>corr</sub>*) of CNTs/CuCrY was better than that of CNTs/CuCr. These indicate that Y addition improves corrosion resistance of the material in a salt water [33]. Protection efficiency (PE) was obtained based on the measured *I<sub>corr</sub>* values using the following equation [34]:

$$PE = \frac{I_{corr}(\text{CNTs/CuCrY}) - I_{corr}(\text{CNTs/CuCr})}{I_{corr}(\text{CNTs/CuCrY})} \times 100\% \quad (1)$$

According to this formula, PE (compared with CNTs/CuCr and CNTs/CuCrY) is 53.28%. The corrosion resistance of CNTs/CuCrY was better than that of CuCrY. Thus, the incorporation of Y and CNTs effectively improved corrosion





**Figure 3:** (a) Survey, (b) Cu 2p and (c, d) C 1s XPS spectra of CNTs/CuCr and CNTs/CuCrY composite powders, respectively, (e) Y 3d XPS spectra of CNTs/CuCrY composite powders.

resistance of the material. The corrosion rate (CR) was estimated from the corrosion current values using the standard equation [Eq. (2)] [35, 36]:

$$CR = \frac{K \times I_{corr} \times M}{z \times \rho} \quad (2)$$

where  $K$  is the corrosion rate constant equal to  $3.27 \times 10^{-3}$  mm g/( $\mu$ A cm year),  $M$  is the Cu atomic weight equal

to 63.5,  $z$  is the valency equal to 2, and  $\rho$  is the density of the corroding metal equal to  $8.97$  g/cm<sup>3</sup>.

Electrochemical parameters obtained from polarization curves are summarized in Table II. CNTs/CuCrY composites exhibited significantly improved corrosion resistance than CNTs/CuCr composites. Typically, impurities act as a cathode and Cu acts as an anode. Thus, the contamination of Cu can negatively affect corrosion resistance. After Y incorporation,

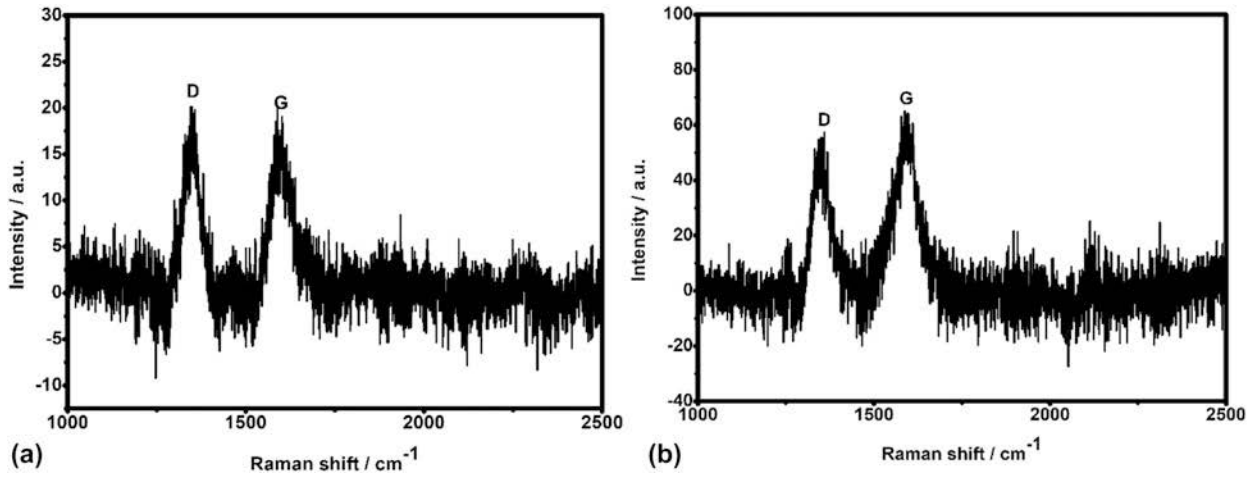


**Figure 4:** Raman spectra of (a) CNTs/CuCr and (b) CNTs/CuCrY composites.

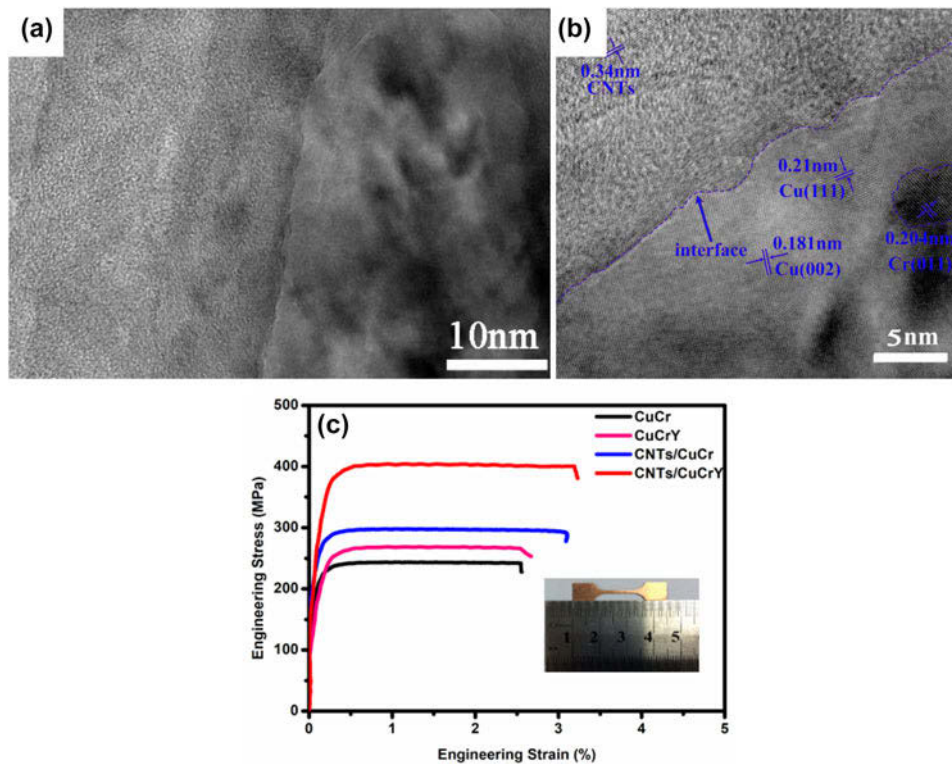


**Figure 5:** Low-magnification (a) and high-magnification (b) TEM images of the CNTs/CuCrY interface. (c) Tensile stress–strain curves for CuCr, CuCrY, CNTs/CuCr, and CNTs/CuCrY composites.

**TABLE I:** Tensile strength and conductivity of CuCr, CuCrY, CNTs/CuCr, and CNTs/CuCrY composites.

Sample	Tensile strength (MPa)	Conductivity (%ACS)
CuCr	243.1	83.1
CuCrY	267.3	85.8
CNTs/CuCr	297.4	86.7
CNTs/CuCrY	402.1	90.9

impurities were eliminated, purifying Cu matrix, reducing active area of the cathode, and suppressing microelectrolytic corrosion. Y can also act as a barrier against further corrosion [19, 37, 38].

Figure 7 displays SEM micrographs of worn surfaces of the four materials after sliding against stainless steel at 10 N load and 0.03 m/s sliding speed. The surface of worn CuCr

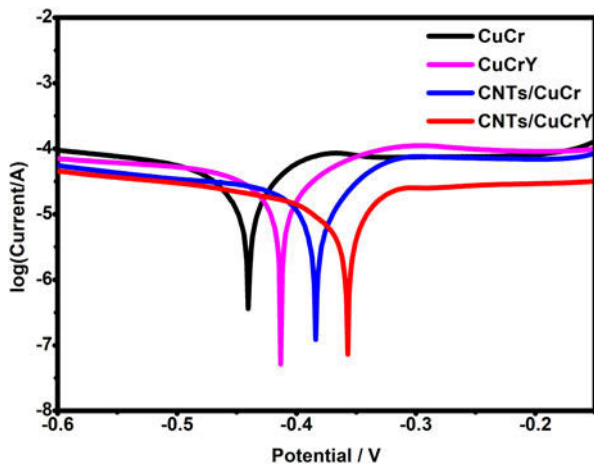


**Figure 6:** Tafel test curves for CuCr, CuCrY, CNTs/CuCr, and CNTs/CuCrY composites in 3.5 wt% NaCl solution.

**TABLE II:** Corrosion-related electrochemical characteristics of CuCr, CuCrY, CNTs/CuCr, and CNTs/CuCrY composites in 3.5 wt% NaCl solution.

Sample	$E_{corr}$ (V)	$I_{corr}$ ( $\mu\text{A}/\text{cm}^2$ )	CR (mm/year)
CuCr	-0.44	35.91	0.416
CuCrY	-0.41	26.52	0.307
CNTs/CuCr	-0.39	21.04	0.244
CNTs/CuCrY	-0.36	9.83	0.114

composites exhibited signs of severe plastic deformation such as grooves and tear [see Figs. 7(a) and 7(b)]. However, less of these features were observed on the worn surfaces of CuCrY composites [Figs. 7(c) and 7(d)], which we attributed to Y incorporation. Y reacts with Cu impurities changing its state from a fusible eutectic one to a high melting state, which increases plasticity of the material. At the same time, the friction properties of CNTs/CuCr and CNTs/CuCrY were greatly improved. CNTs play a self-lubricating role in the matrix. During the friction and wear processes, carbon film forms on the wear surface reducing the wear [39, 40]. The friction coefficients of CNTs/CuCr and CNTs/CuCrY composites were 0.5 and 0.3, respectively. Thus, the incorporation of Y reduced the friction coefficient by 40%. This is because, on one hand, Y addition increased plasticity of the matrix. On the other hand, CNTs/CuCrY contained more CNTs [Fig. 2(e)]. Thus, this composite had more significant self-lubricating effect and reduced friction coefficients [41, 42].

## Conclusions

We synthesized Cu-based CNT composites using Cr catalyst with and without Y presence. The addition of Y improved aging precipitation of catalytic Cr particles and enhanced properties of composites. Our novel and innovative approach addresses dispersion issues of CNTs in CNTs/Cu composites.

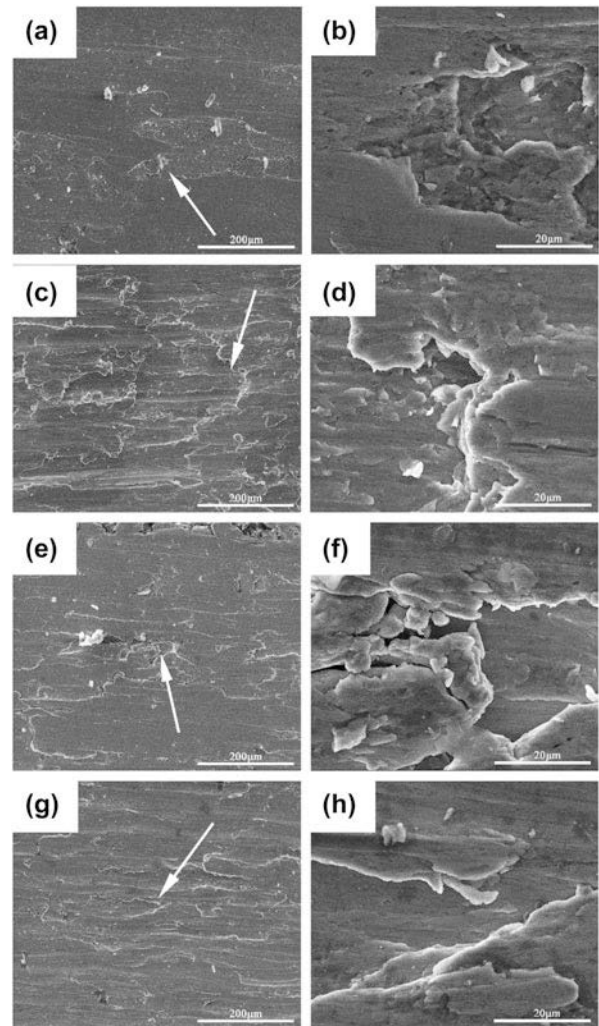


**Figure 7:** SEM micrographs of surfaces of (a), (b) CuCr, (c), (d) CuCrY, (e), (f) CNTs/CuCr, and (g), (h) CNTs/CuCrY composites after friction and wear tests at 10 N load and 0.03 m/s sliding speed.

Main results and conclusions of this work are mentioned below.

- (1) The addition of Y not only promoted performance of catalytic Cr particles but also purified Cu surface, which helped to obtain higher quality CNTs without defects and amorphous carbon deposits. These CNTs were also more evenly distributed and had smoother walls.
- (2) The presence of Y also resulted in higher CNT yield, which in turn increased (i) tensile strength of CNTs/CuCr composites from 297.4 (without Y presence) to 402.1 MPa, (ii) hardness from 93.6 (without Y presence) to 102.5 HV, and (iii) electrical conductivity from 86.7% (without Y presence) to 90.9% IACS.
- (3) CNTs/CuCrY composites demonstrated  $E_{corr}$  increase from  $-0.39$  to  $0.36$  V and corrosion resistance ( $I_{corr}$ ) decrease from  $21.04$  to  $9.83 \mu\text{A}/\text{cm}^2$ . As a result, CR

dropped from 0.244 mm/year to 0.114 mm/year in comparison to the CNTs/CuCr composites.

- (4) The addition of Y also reduced friction coefficients of the Cu-based CNT composites from 0.5 (for CNT/CuCr composites) to 0.3. Wear resistance was also enhanced.

## Experimental

### Preparation of CNTs/CuCr and CNTs/CuCrY composites

CuCr and CuCrY alloy powders with average size of 200 mesh were obtained from Guoyao Group Reagent Net. The concentrations of Cr and Y were 0.6 and 0.1 wt%, respectively, relative to the total Cu weight.

12 g of CuCr or CuCrY alloy powders were placed into a tube furnace. The flow of each gas was measured in standard cubic centimeters per minute (sccm). Powders were held at 860 °C for 60 min and then were additionally aged at 500 °C for 120 min under constant flow of 1300 sccm of H<sub>2</sub> (used as a reducing gas) and 1650 sccm of Ar (used as protective gas). After that, C<sub>2</sub>H<sub>4</sub> gas was added into the system as a carbon source to synthesize CNTs/CuCr and CNTs/CuCrY composite powders. Synthesis of these composite powders was performed at 800 °C for 60 min.

Then, these CNTs/CuCr and CNTs/CuCrY composites were placed in a graphite mold (with an inner diameter of

30 mm) and heated in a plasma sintering furnace (KCE-FCT HP D 6-SI) at 100 °C/min heating rate and 30 MPa pressure. The reaction was conducted at 900 °C for 10 min. At the end of the reaction, CNTs/CuCr and CNTs/CuCrY composites were obtained. This experimental process is depicted in Fig. 8. Composite materials were hot rolled at 850 °C till 60% deformation to increase their density.

### Characterization

Morphology and distribution of the catalysts and CNTs were characterized by scanning electron microscopy (SEM) using QUANTA FEG 450 (FEI Corporation, Hillsboro, Oregon). Phase composition were characterized by X-ray diffraction (XRD) using D8 ADVANCE instrument (Zwick Corporation, Germany). Microstructures of the composites were analyzed by field emission transmission electron microscopy (FE-TEM) using Tecnai G2 F30 (FEI Corporation, Hillsboro, Oregon). Elemental composition and chemical bonds were characterized by X-ray photoelectron spectroscopy (XPS) using Thermo ESCALAB 250 (Thermo Fisher Scientific Corporation, Waltham, Massachusetts). Quality of the CNTs was assessed using Raman spectroscopy (Raman Station 400F) equipped with Ar laser with 532 nm wavelength as the excitation source. Tensile strength, hardness, and electrical conductivity of the composites were tested by a micro-tensile tester (using Zwick Precision Line Vario; Zwick Corporation, Germany),

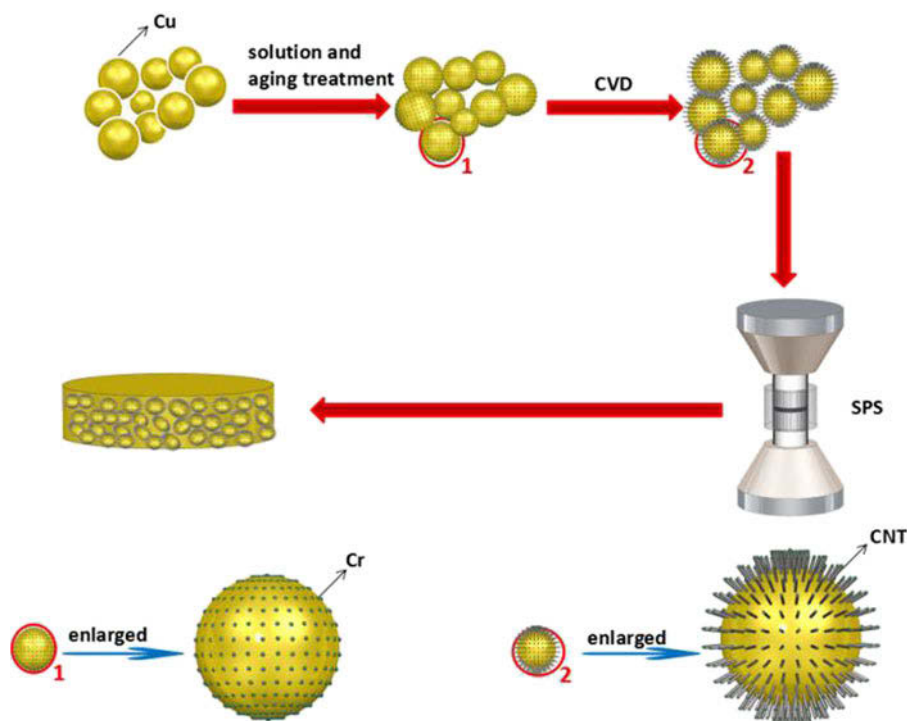


**Figure 8:** Schematics of the composite powders and composite materials preparation.



a microhardness tester (using HX-1000TM/LCD; Zwick Corporation, Germany), and a digital metal conductivity tester D60K, respectively. Corrosion resistance and friction as well as wear properties of the composites were analyzed using electrochemical workstations (CHI 660D, CHI 1140C) and friction wearer (HIIT-2II), respectively.

## Acknowledgments

This work was supported by the National Natural Science Foundation of China (Grant No. 51201107), National Key R & D Program of China (Grant No. 2017YFB0306405), and Key Project of Shanghai Municipal Science and Technology Commission (Grant No. 10JC1411800).

## References

- X.Z. Zhang, Z.K. Huang, G.W. Liu, T.T. Wang, J. Yang, H. C. Shao, and G.J. Qiao: Wetting and brazing of Ni-coated WC-8Co cemented carbide using the Cu-19Ni-5Al alloy as the filler metal: Microstructural evolution and joint mechanical properties. *J. Mater. Res.* **33**, 1671 (2018).
- L.Q. Xiong, K.W. Liu, J. Shuai, Z.C. Hou, Z. Lin, and W.Z. Li: Toward high strength and high electrical conductivity in super-aligned carbon nanotubes reinforced copper. *Adv. Eng. Mater.* **20**, 1700805 (2017).
- S.C. Tjong: Recent progress in the development and properties of novel metal matrix nanocomposites reinforced with carbon nanotubes and graphene nanosheets. *Mater. Sci. Eng., R* **74**, 281 (2013).
- S.R. Bakshi, D. Lahiri, and A. Agarwal: Carbon nanotube reinforced metal matrix composites—A review. *Metall. Rev.* **55**, 41 (2010).
- S. Cho, K. Kikuchi, E. Lee, M. Choi, I. Jo, S.B. Lee, S.K. Lee, and A. Kawasaki: Chromium carbide/carbon nanotube hybrid structure assisted copper composites with low temperature coefficient of resistance. *Sci. Rep.* **7**, 14943 (2017).
- W.M. Daoush, B.K. Lim, C.B. Mo, H.N. Dong, and S.H. Hong: Electrical and mechanical properties of carbon nanotube reinforced copper nanocomposites fabricated by electroless deposition process. *Mater. Sci. Eng., A* **513**, 247 (2009).
- A.K. Shukla, N. Nayan, S.V.S.N. Murty, K. Mondal, S. C. Sharma, K.M. George, and S.R. Bakshi: Processing copper-carbon nanotube composite powders by high energy milling. *Mater. Charact.* **84**, 58 (2013).
- M. Estili and A. Kawasaki: An approach to mass-producing individually alumina-decorated multi-walled carbon nanotubes with optimized and controlled compositions. *Scr. Mater.* **58**, 906 (2008).
- M. Rahimian, N. Ehsani, N. Parvin, and H.R. Baharvandi: The effect of particle size, sintering temperature and sintering time on the properties of Al-Al<sub>2</sub>O<sub>3</sub> composites, made by powder metallurgy. *J. Mater. Process. Technol.* **209**, 5387 (2009).
- J.W. Qian, Z.Y. Zhao, Z.G. Shen, G.L. Zhang, Z.J. Peng, and X. L. Fu: A large scale of CuS nano-networks: Catalyst-free morphologically controllable growth and their application as efficient photocatalysts. *J. Mater. Res.* **30**, 3746 (2015).
- J. Kong, H.T. Soh, A.M. Cassell, C.F. Quate, and H.J. Dai: Synthesis of individual single-walled carbon nanotubes on patterned silicon wafers. *Nature* **395**, 878 (1998).
- N. Inami, M.A. Mohamed, E. Shikoh, and A. Fujiwara: Synthesis-condition dependence of carbon nanotube growth by alcohol catalytic chemical vapor deposition method. *Sci. Technol. Adv. Mater.* **8**, 292 (2007).
- J.L. Kang, P. Nash, J.J. Li, C.S. Shi, and N.Q. Zhao: Achieving highly dispersed nanofibres at high loading in carbon nanofibre-metal composites. *Nanotechnology* **20**, 235607 (2009).
- Y. Jin, K. Adachi, T. Takeuchi, and H.G. Suzuki: Ageing characteristics of Cu-Cr in situ composite. *J. Mater. Sci.* **33**, 1333 (1998).
- D.Z. Florio and R. Muccillo: Sintering of zirconia-yttria ceramics studied by impedance spectroscopy. *Solid State Ionics* **123**, 301 (1999).
- J.L. Kang, J.J. Li, X.W. Du, C. Shi, N.Q. Zhao, and P. Nash: Synthesis of carbon nanotubes and carbon onions by CVD using a Ni/Y catalyst supported on copper. *Mater. Sci. Eng., A* **475**, 136 (2008).
- T. Du and L.G. Dong: Thermodynamics and phase equilibrium of Cu-Ce-O, Cu-Ce-S, Cu-Ce-O-S liquid solutions. *J. Iron Steel Res. Int.* **1**, 10 (1995).
- Z. Rdzawski: Effect of rare-earth metals addition on microstructure and properties of selected copper alloys. *Arch. Metall. Mater.* **59**, 641 (2014).
- H.H. Li, X.Q. Sun, S.Z. Zhang, Q.Y. Zhao, and G.Z. Wang: Application of rare-earth element Y in refining impure copper. *Int. J. Miner., Metall. Mater.* **22**, 453 (2015).
- H.Z. Li, X.P. Liang, F.F. Li, F.F. Guo, Z. Li, and X.M. Zhang: Effect of Y content on microstructure and mechanical properties of 2519 aluminum alloy. *Trans. Nonferrous Met. Soc. China* **17**, 1194 (2007).
- X.H. Wang, Y. Liang, J.T. Zou, S.H. Liang, and Z.K. Fan: Effect of rare earth Y addition on the properties and precipitation morphology of aged Cu-Cr-Ti lead frame alloy. *Adv. Mater. Res.* **97**, 578 (2010).
- M. Endo and H.W. Kroto: Formation of carbon nanofibers. *Phys. Chem.* **96**, 6941 (1992).
- J. Kong, A.M. Cassell, and H. Dai: Chemical vapor deposition of methane for single-walled carbon nanotubes. *Chem. Phys. Lett.* **292**, 567 (1998).
- Zhongguo Keji Lunwen Zaixian: Study on in situ synthesis of carbon nano morphologies by Fe/Y catalyst on copper. Available

- at: <http://www.paper.edu.cn/releasepaper/content/201006-377>  
(accessed January 24, 2019).
25. **Z.Y. Yang, L.D. Wang, Z.D. Shi, M. Wang, Y. Cui, B. Wei, S. C. Xu, Y.P. Zhu, and W.D. Fei:** Preparation mechanism of hierarchical layered structure of graphene/copper composite with ultrahigh tensile strength. *Carbon* **127**, 329 (2018).
  26. **Q. Zhang, C. Cai, J.W. Qin, and B.Q. Wei:** Tunable self-discharge process of carbon nanotube based supercapacitors. *Nano Energy* **4**, 14 (2014).
  27. **A. Pulido, P. Concepcion, M. Boronat, C. Botas, and A. Corma:** Reconstruction of the carbon  $sp^2$  network in graphene oxide by low-temperature reaction with CO. *J. Mater. Chem.* **22**, 51 (2011).
  28. **P. Gao, F. Li, N. Zhao, F.K. Xiao, W. Wei, L.S. Zhong, and Y. H. Sun:** Influence of modifier (Mn, La, Ce, Zr, and Y) on the performance of Cu/Zn/Al catalysts via hydrotalcite-like precursors for CO<sub>2</sub> hydrogenation to methanol. *Appl. Catal., A* **468**, 442 (2013).
  29. **S.A. Chernyak, A.S. Ivanov, K.I. Maslakov, A.V. Egorov, Z. Shen, S.S. Savilov, and V.V. Lunin:** Oxidation, defunctionalization and catalyst life cycle of carbon nanotubes: A Raman spectroscopy view. *Phys. Chem. Chem. Phys.* **19**, 2276 (2017).
  30. **M.F. Ran, W.J. Sun, Y. Liu, C. Wei, and C.F. Jiang:** Functionalization of multi-walled carbon nanotubes using water-assisted chemical vapor deposition. *J. Solid State Chem.* **197**, 517 (2013).
  31. **C. Ke, C.C. Jia, L.K. Jiang, and W.S. Li:** Improvement of interface and mechanical properties in carbon nanotube reinforced Cu–Cr matrix composites. *Mater. Des.* **45**, 407 (2013).
  32. **E.N. Popova, I.L. Deryagina, M.V. Polikarpova, D. C. Novosilova, and A.E. Vorobyova:** Effect of interfaces and Cr diffusion on stabilizing Cu conductivity in Nb<sub>3</sub>Sn-strands. *Defect Diffus. Forum* **335**, 241 (2013).
  33. **Y. Jafari, S.M. Ghoreishi, and M. Shabani-Nooshabadi:** Polyaniline/graphene nanocomposite coatings on copper: Electropolymerization, characterization, and evaluation of corrosion protection performance. *Synth. Met.* **217**, 220 (2016).
  34. **M. Shabani-Nooshabadi, M. Mollahoseiny, and Y. Jafari:** Electropolymerized coatings of polyaniline on copper by using the galvanostatic method and their corrosion protection performance in HCl medium. *Surf. Interface Anal.* **46**, 472 (2014).
  35. **Y. Raghupathy, K.A. Natarajan, and C. Srivastava:** Anti-corrosive and anti-microbial properties of nanocrystalline Ni–Ag coatings. *Mater. Sci. Eng., B* **206**, 1 (2016).
  36. **A. Kamboj, Y. Raghupathy, M.Y. Rekha, and C. Srivastava:** Morphology, texture and corrosion behavior of nanocrystalline copper–graphene composite coatings. *JOM* **69**, 1 (2017).
  37. **G.Y. Lin, W. Yang, Y.C. Wan, P.J. Tang, B. Wei, and S. H. Zhang:** Influence of rare earth elements on corrosion resistance of BFe10-1-1 alloys in flowing marine water. *J. Rare Earths* **27**, 259 (2009).
  38. **F. Rosalbino, R. Carlini, F. Soggia, G. Zanicchi, and G. Scavino:** Influence of rare earth metals addition on the corrosion behaviour of copper in alkaline environment. *Corros. Sci.* **58**, 139 (2012).
  39. **Y. Gao, J.C. Jie, P.C. Zhang, J. Zhang, T.M. Wang, and L.T. Ju:** Investigation of the wear behavior of high strength and high conductivity Cu–Cr–Zr alloy under dry sliding. *Mater. Sci. Forum* **817**, 661 (2015).
  40. **B.B. Chen, Y. Jin, Q. Zhang, H. Hong, H.P. Li, T. Hua, and C. S. Li:** Tribological properties of copper-based composites with copper coated NbSe<sub>2</sub>, and CNT. *Mater. Des.* **75**, 24 (2015).
  41. **J.H. Nie, X. Jia, C.C. Jia, Y. Li, Y.F. Zhang, and N. Shi:** Friction and wear properties of copper matrix composites reinforced by tungsten-coated carbon nanotubes. *Rare Met.* **30**, 657 (2011).
  42. **Y.L. Xin, Z.X. Xiong, N. Fei, and J.B. Xiao:** Properties of copper/graphite/carbon nanotubes composite reinforced by carbon nanotubes. *Rare Met.* **32**, 278 (2013).